X-Ray Absorption Signatures of the Molecular Environment in Water and Ice

Wei Chen,[1] Xifan Wu,[2] and Roberto Car[1,2,3,*]

[1]Department of Physics, Princeton University, Princeton, New Jersey 08544, USA
[2]Department of Chemistry, Princeton University, Princeton, New Jersey 08544, USA
[3]Princeton Institute for the Science and Technology of Materials, Princeton University, Princeton, New Jersey 08544, USA

(Received 21 September 2009; published 30 June 2010)

The x-ray absorption spectra of water and ice are calculated with a many-body approach for electron-hole excitations. The experimental features, including the effects of temperature change in the liquid, are reproduced from configurations generated by *ab initio* molecular dynamics. The spectral difference between the solid and the liquid is due to two major short-range order effects. One, due to breaking of hydrogen bonds, enhances the pre-edge intensity in the liquid. The other, due to a nonbonded molecular fraction in the first coordination shell, affects the main spectral edge in the conversion of ice to water. This effect may not involve hydrogen bond breaking as shown by experiment in high-density amorphous ice.

DOI: 10.1103/PhysRevLett.105.017802 PACS numbers: 61.25.Em, 61.05.cj, 71.15.Pd, 82.30.Rs

The nature of the hydrogen-bond (H-bond) network in water continues to be at the center of scientific debate [1]. A few years ago, high-resolution x-ray absorption spectra (XAS) probed the local order of liquid and crystalline water phases, including the effect of temperature in the liquid [2]. These experiments stirred a storm of controversy because of their interpretation suggesting that a majority ($>80\%$) of H bonds are broken in the liquid [2]. This would imply dominance of chains and rings of H bonds, in stark contrast to the conventional near-tetrahedral picture supported by diffraction [3], thermodynamic, and spectroscopic data [4,5]. The broken H-bond fraction was estimated from the intensity of the pre-edge peak, which is prominent in the liquid and was believed to be absent in bulk ice. X-ray Raman spectra, however, showed that the pre-edge feature is present, albeit with different intensity, not only in the liquid, but also in hexagonal (Ih), cubic (Ic), low-density amorphous (LDA), and high-density amorphous (HDA) ice [6]. This experiment also reported that water and HDA ice have spectra with the near edge more prominent than the post-edge, while the opposite occurs in Ih, Ic, and LDA ice. This is puzzling given that both LDA and HDA ice are disordered structures with an insignificant fraction of broken H bonds. Spectral calculations, based on electronic density-functional theory (DFT) and near-tetrahedral liquid models, correctly predicted the presence of three spectral features in ice and water and associated the enhancement of the pre-edge intensity to broken H bonds [7–10]. However, the agreement with experiment was only semiquantitative, and the calculations did not identify the cause of the significant changes in near- and post-edge spectra. These effects were generically attributed to disorder [8], but this does not explain why LDA and HDA ice show opposite behavior [6]. Finally, no attempt was made to discuss the effect of temperature observed in the liquid spectra [2,11–13].

In this paper, we use liquid structures generated by *ab initio* molecular dynamics (MD) [14] to compute x-ray spectra by adopting the final state rule [15,16] within a many-body formalism for electronic excitations [17]. Our calculations reproduce quantitatively the experimental spectra and their temperature dependence, supporting prior theoretical claims that the spectra are fully consistent with the conventional near-tetrahedral model of the liquid [8]. We associate the x-ray features to molecular excitons strongly influenced by the medium. Broken H bonds do enhance the pre-edge intensity [2], but the difference between water and ice is also due to other factors associated with liquid disorder and does not require an exceedingly large fraction of broken bonds [8]. A novel result is the finding that the large reduction of post-edge intensity from ice to water correlates with the substantial weakening in the liquid of a prominent feature of the ice density of states. We attribute this behavior to a nonbonded molecular fraction in the first coordination shell of the liquid. The short-range order (SRO) of water reflects the partial collapse of the H-bond network, but diffraction data [18] suggest that a nonbonded molecular fraction should also be present, without broken bonds, in HDA ice. We argue that this could explain the weak post-edge feature of this system.

Our approach is an approximation to the Bethe-Salpeter equation for electron-hole excitations [17], which was applied successfully to compute the optical absorption spectra of Ih ice [19] and liquid water [20]. Here we neglect the dynamics of the oxygen 1s core hole, which is localized and long-lived on the time scale of the absorption process. Then the Bethe-Salpeter equation reduces to a quasiparticle equation for the excited electron in the presence of the frozen core hole and the sea of the other electrons [16]. We solve this equation within the static Coulomb-hole and screened exchange (COHSEX) approximation [14,17]. In this approach the local exchange-correlation potential of DFT is replaced by a nonlocal self-energy operator, which we evaluate in real space using maximally localized Wannier functions [14,21].

In Fig. 1, we compare calculated and experimental spectra [2] of ice and water. The spectra are aligned at the onset [14,22], and all the theoretical curves are multiplied by the scaling factor that adjusts the intensity of the near-edge water peak (at $T = 363$ K) to the corresponding experimental value (at STP). We use Gaussian broadening with a full width at half maximum of 0.6 and 0.4 eV, for ice and water, respectively, to remove discreteness from the calculated spectra [23] and to account for quasiparticle lifetime and other broadening effects ignored in the calculation. The liquid spectra are averages of the excitations of the individual molecules (32) in the simulation cell. A representative MD snapshot was used at each temperature [14]. DFT calculations showed that averaging over more snapshots had minor effect, in agreement with Ref. [8]. In the simulation the molecules are approximately tetrahedrally coordinated with ~7% and ~11% broken H bonds at $T = 330$ K and $T = 363$ K, respectively, according to the criteria of Ref. [24], or with ~14% and ~18% broken H bonds, respectively, according to the criteria of Ref. [2].

The three main experimental features, pre-edge (533–536 eV), near edge (537–539 eV), and post-edge (from 539 eV and beyond), are well reproduced in terms of position, intensity, and spectral width. By contrast, previous DFT calculations, using excited- [8] or full-core-hole [7] potentials, underestimated the overall spectral width by ~2 eV or more, respectively, with corresponding shifts in the relative peak positions. Somewhat better spectral widths were obtained in half-core-hole calculations [10,25], but this approach gave worse agreement in the pre- and near edge [7,9]. These inaccuracies are caused by the local DFT exchange-correlation potential that acts equally on all the excited states [26]. By contrast the nonlocal self-energy operator causes higher energy states to experience reduced exchange effects, i.e., a reduced attractive potential, for an overall increase of the spectral width. The agreement between theory and experiment is good in the liquid, in which we average over a representative set of local oxygen configurations. In ice instead we used the classical $T = 0$ molecular geometry without proton disorder. That and the $k = 0$ approximation in the spectral calculation [23] are responsible for the splitting of the post-edge feature into two relatively sharp peaks, at lower and higher energy, respectively, compared to the single, broader, experimental feature [28]. In the liquid [Fig. 1(c) and 1(d)], a temperature increase enhances pre- and near-edge at the expense of post-edge intensity. Qualitatively, the same effect occurs in the transition from ice to water [2]. Comparison of theoretical and experimental difference spectra in Fig. 1(d) shows that the small effects of a temperature change are well reproduced, as illustrated by the isosbestic point that falls at 538.4 eV in the calculation and at 538.8 eV in the experiment. Such a close correspondence in a derivative property would be unlikely barring a good correspondence in the molecular trends. Similar temperature effects in the pre- and post-edge features were also found in nanodroplet experiments [11].

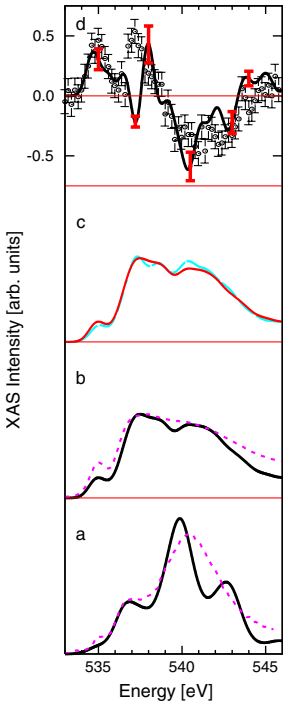

FIG. 1 (color online). Calculated and experimental [2] XAS spectra. From bottom to top. (a) Ice: Full line—theory, ice Ic; dashed line—experiment, ice Ih, at 95 K. (b) Water: Full line—theory at 363 K; dashed line—experiment at 290 K. (c) Theoretical spectra for water at two different temperatures: blue line, at 330 K, and red line, at 363 K. (d) Difference spectra: Theory and experiment (data points with error bars). Details on the alignment and on the theoretical error bars (red) are given in the supporting online material [14]. As the temperature difference in the experiment ($\Delta T = 65$ K) was nearly double that in the calculation ($\Delta T = 33$ K), the theoretical data are magnified by a factor of 10, while the experimental data are magnified by a factor of 5 instead of by the factor of 10 used in Ref. [2]. Linear dependence on temperature is to be expected for a temperature change small on the energy scale of the structural changes.

The calculated pre-edge is weaker than experiment in both water and ice, but the intensity ratio is reasonably reproduced. This reflects approximations in the calculation. For example, vibrational (finite T and zero-point motion) effects in ice should enhance the pre-edge feature. Pre-edge underestimation could also result from the assumption of a fully screened core hole. Moreover, network distortion and fraction of broken bonds in water simulations with classical nuclei and Perdew-Burke-Ernzerhof exchange correlation [29] could be underestimated in spite of a temperature ~60 K higher than experiment [14,30].

In Fig. 2, we report the COHSEX quasiparticle wave functions of representative pre-edge, near-edge, and post-edge states of ice and water, and the three lowest energy features of the monomer absorption spectrum. The latter were obtained by setting the screening $\epsilon = 1$ in the COHSEX equations [14] resulting in a XAS spectrum close to that obtained in Ref. [31] within time-dependent Hartree-Fock theory. The monomer orbitals are antibond-

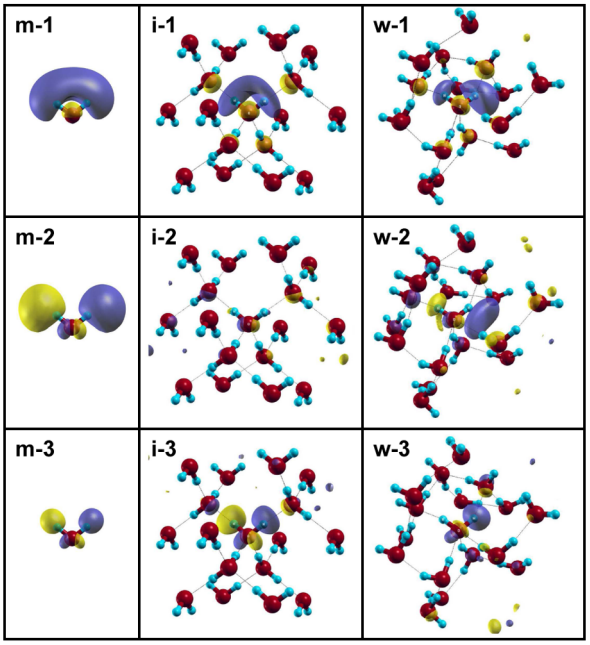

FIG. 2 (color online). Excited electron state in the presence of a core hole on the central oxygen atom. The calculation is at the Hartree-Fock level for the monomer (m) and at the COHSEX level for ice Ic (i) and water (w). 1: Pre-edge; 2: near edge; 3: post-edge. Molecules up to the second coordination shell are shown for ice and water. The color difference in the plots corresponds to a difference in the sign of the wave function.

ing states of $4a_1$, $2b_2$, and $3b_2$ symmetry, respectively. The similarity of condensed and gas phase orbitals suggests that the XAS features in ice and water should be attributed to molecular excitons strongly perturbed by the environment.

We assign the pre-edge to a bound exciton whose electron orbital is similar to that of the valence exciton that marks the onset of optical transitions in ice [19]. Although localized on the excited molecule, this orbital has significant weight also on the four nearest molecules, but the degree of localization may depend on our approximations, such as, e.g., using a fully screened core hole and partially neglecting local field effects. The intact H-bond network of ice enhances the symmetry and reduces the p character of the excited quasielectron on oxygen, lowering the dipolar transition amplitude and the pre-edge intensity, but the effect is not sufficient to make the feature disappear. This would require the distinction between donor and acceptor bonds to vanish as in ice X, a stable form of ice under extreme pressure [32]. From detailed analysis we find that, while on average configurations with broken H bonds contribute more to the pre-edge intensity than configurations with intact bonds, some distorted tetrahedral configurations can be equally effective. Distortion and fraction of broken H bonds increase with temperature, enhancing the pre-edge intensity.

The near and post-edge features correspond to more delocalized states and originate from several closely spaced levels in our supercell calculations, consistent with the assignment to exciton resonances. While in the monomer and the liquid higher energy states are less localized, the opposite happens in ice, as also reflected in the corresponding relative intensities of near- and post-edge peaks. This phenomenon is not caused by the transition matrix element, as both near- and post-edge resonances have strong oxygen p character, but originates from the density of states (DOS). This is illustrated in Fig. 3, which depicts the DOS of water and ice (in the absence of core hole within DFT). The conduction DOS of ice has a sharp peak at $\sim$8 eV above the band edge corresponding to antibonding molecular orbitals of b_2 symmetry. These orbitals have lobes protruding from the covalently bonded hydrogens and on the lone pair side of oxygen. In ice the antibonding b_2 state of a molecule does not overlap with the corresponding state of an adjacent molecule, originating a sharp peak in the DOS (Fig. 3). Because of the distinction between antibonding and bonding directions, overlap between antibonding states of H-bonded molecules is effectively forbidden. By contrast, when a nonbonded molecule is in the first coordination shell, overlap occurs, often involving the antibonding H lobes of two adjacent nonbonded molecules (Fig. 3). A substantial structural change is necessary for that to happen. In the liquid it follows from the partial collapse of the H-bond network. Orbital interaction broadens substantially the peak in the DOS (Fig. 3). As a consequence, post-edge intensity is reduced and oscillator strength is transferred to the near edge. This happens when ice melts and, to a lesser extent, when the temperature is raised in the liquid. Interestingly, the simulations of Ref. [8] found that, when the liquid is quenched to form a glass, substantial post-edge intensity is recovered together with good tetrahedral coordination, albeit in a noncrystalline lattice. This structure should mimic LDA ice, which is obtained experimen-

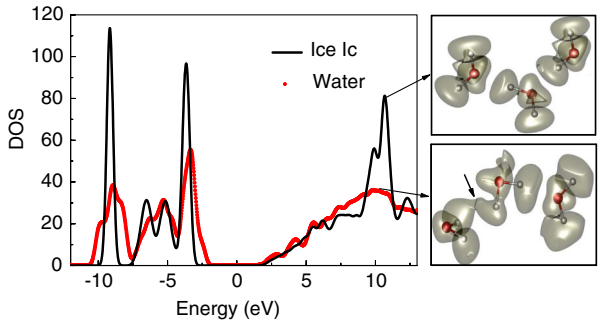

FIG. 3 (color online). Electronic DOS of ice (Ic) and water, calculated with a $4 \times 4 \times 4$ k-point mesh (ice) and at $k = 0$ (water) with Gaussian broadening of 0.3 eV. The conduction states have positive energy. The insets show a central tagged molecule and two adjacent molecules in ice (top) and water (bottom). Also plotted is the integrated local DOS in correspondence with the DOS peaks. The bottom inset shows overlap, indicated by an arrow, between the antibonding density of the nonbonded molecule on the left and the central molecule, while no overlap occurs between the latter and the bonded molecule at its right. See also Ref. [14].

tally by quenching the liquid. LDA ice has SRO close to cubic and hexagonal ice [18], and the corresponding main x-ray edges are very similar [6]. On the other hand, HDA ice, which is obtained by pressure amorphization, sports a main edge similar to the liquid with a pre-edge closer to the crystal [6]. The latter is consistent with the absence of broken bonds [18]. Yet HDA has SRO different from crystalline ice, and actually closer to the liquid, due to the presence of an additional nonbonded molecule, on average, at nontetrahedral locations within the first coordination shell [18]. Arguably, this could be the reason for the similarity of the main edges of HDA ice and water, which both have molecular density *higher* than crystalline ice. In our liquid snapshots more than 10% of the molecules have overlapping antibonding orbitals. Interestingly, more than 60% of these molecules have five neighbors. Some of these local configurations correspond to a tetrahedrally bonded central molecule (2 donors and 2 acceptors) with a nonbonded molecule additionally present in the coordination shell. Occasionally, the latter molecule may also be tetrahedrally bonded, resulting in a local configuration similar to those suggested for HDA ice in Ref. [18].

In conclusion, spectral calculations beyond ground-state DFT bear close correspondence to experiment. Our study confirms the sensitivity of the XAS spectra to SRO modifications due to structural transitions and temperature changes. H-bond breaking mainly affects the pre-edge while the near and post-edges are sensitive to an increase of coordination due to a nonbonded molecular fraction. Our work further confirms that the XAS spectrum of water is consistent with the conventional near-tetrahedral picture. The calculated effects of a temperature change in the liquid are illuminating. Theory automatically guarantees the relative normalization of the spectra at different temperatures, a condition that may not be straightforward to enforce in experimental spectra [12,13]. The agreement of our calculation with the differential spectra of Ref. [2] provides independent support of these data. It also suggests that, in spite of the shortcomings of current DFT approximations, the description of the H-bond network provided by *ab initio* MD is fundamentally correct and can capture molecular trends with surprising accuracy. Finally, we note that recent x-ray emission spectra of liquid water were interpreted in terms of two coexisting local environments, one low coordinated and the other tetrahedral [33–35]. We are unable to directly address this issue as our calculation is limited to XAS, but we note that water structures from *ab initio* MD do not seem to support a two-liquid hypothesis.

We acknowledge support from the Department of Energy under Grant No. DE-FG02-05ER46201 and from the NSF under Grant No. CHE-0956500. We thank G. Galli, A. Nilsson, and L. G. M. Pettersson for useful discussions. The calculations were performed at the National Energy Research Scientific Computing Center, which is supported by the Department of Energy under Contract No. DE-AC02-05CH11231.

*rcar@princeton.edu

[1] P. Ball, Nature (London) **452**, 291 (2008).
[2] P. Wernet *et al.*, Science **304**, 995 (2004).
[3] T. Head-Gordon and M. E. Johnson, Proc. Natl. Acad. Sci. U.S.A. **103**, 7973 (2006).
[4] D. S. Eisenberg and W. Kauzmann, *The Structure and Properties of Water* (Clarendon, Oxford, 1969).
[5] F. H. Stillinger, Science **209**, 451 (1980).
[6] J. S. Tse *et al.*, Phys. Rev. Lett. **100**, 095502 (2008).
[7] B. Hetényi, F. D. Angelis, P. Giannozzi, and R. Car, J. Chem. Phys. **120**, 8632 (2004).
[8] D. Prendergast and G. Galli, Phys. Rev. Lett. **96**, 215502 (2006).
[9] R. L. C. Wang, H. J. Kreuzer, and M. Grunze, Phys. Chem. Chem. Phys. **8**, 4744 (2006).
[10] M. Iannuzzi, J. Chem. Phys. **128**, 204506 (2008).
[11] J. D. Smith *et al.*, Science **306**, 851 (2004).
[12] A. Nilsson *et al.*, Science **308**, 793a (2005).
[13] J. D. Smith *et al.*, Science **308**, 793b (2005).
[14] See supplementary material at http://link.aps.org/supplemental/10.1103/PhysRevLett.105.017802 for details of methods and calculations.
[15] U. von Barth and G. Grossmann, Phys. Rev. B **25**, 5150 (1982).
[16] J. J. Rehr, J. A. Soininen, and E. L. Shirley, Phys. Scr. **T115**, 207 (2005).
[17] G. Onida, L. Reining, and A. Rubio, Rev. Mod. Phys. **74**, 601 (2002).
[18] J. L. Finney *et al.*, Phys. Rev. Lett. **88**, 225503 (2002).
[19] P. H. Hahn *et al.*, Phys. Rev. Lett. **94**, 037404 (2005).
[20] V. Garbuio *et al.*, Phys. Rev. Lett. **97**, 137402 (2006).
[21] X. Wu, A. Selloni, and R. Car, Phys. Rev. B **79**, 085102 (2009).
[22] Pseudopotential calculations provide only relative core excitation energies, and it is common practice to facilitate comparison with experiment by aligning the calculated spectra to the experimental edge (see Ref. [8]).
[23] All calculations are done at the $k = 0$ point of the supercell Brillouin zone.
[24] A. Luzar and D. Chandler, Phys. Rev. Lett. **76**, 928 (1996).
[25] M. Cavalleri, M. Odelius, A. Nilsson, and L. G. M. Pettersson, J. Chem. Phys. **121**, 10065 (2004).
[26] The importance of nonlocal exchange was underlined in a cluster calculation using a hybrid functional. This improved the pre- and main edge, but failed in the post-edge [27].
[27] G. Brancato, N. Rega, and V. Barone, Phys. Rev. Lett. **100**, 107401 (2008).
[28] We found, at the DFT level of theory, that vibrational broadening and better k-point sampling [8] make the two features merge into a single broader peak.
[29] J. P. Perdew, K. Burke, and M. Ernzerhof, Phys. Rev. Lett. **77**, 3865 (1996).
[30] J. A. Morrone and R. Car, Phys. Rev. Lett. **101**, 017801 (2008).
[31] R. K. Pandey and S. Mukamel, J. Chem. Phys. **124**, 094106 (2006).
[32] R. J. Hemley *et al.*, Nature (London) **330**, 737 (1987).
[33] T. Tokushima *et al.*, Chem. Phys. Lett. **460**, 387 (2008).
[34] O. Fuchs *et al.*, Phys. Rev. Lett. **100**, 027801 (2008).
[35] M. Odelius *et al.*, Phys. Rev. B **79**, 144204 (2009).